DETAILED STUDIES OF

Might the core barrel of a nuclear reactor suffer permanent deformation as a result of a break in an inlet pipe? The question has been examined with coupled fluid- and structural-dynamics computer codes. Shown here are four frames from a computer-generated movie by Rongriego depicting the calculated results. The left of each frame shows the deformation, which has been magnified 200 times for clarity. On the right of each frame color variations indicate the variation of pressure differences across the core barrel.

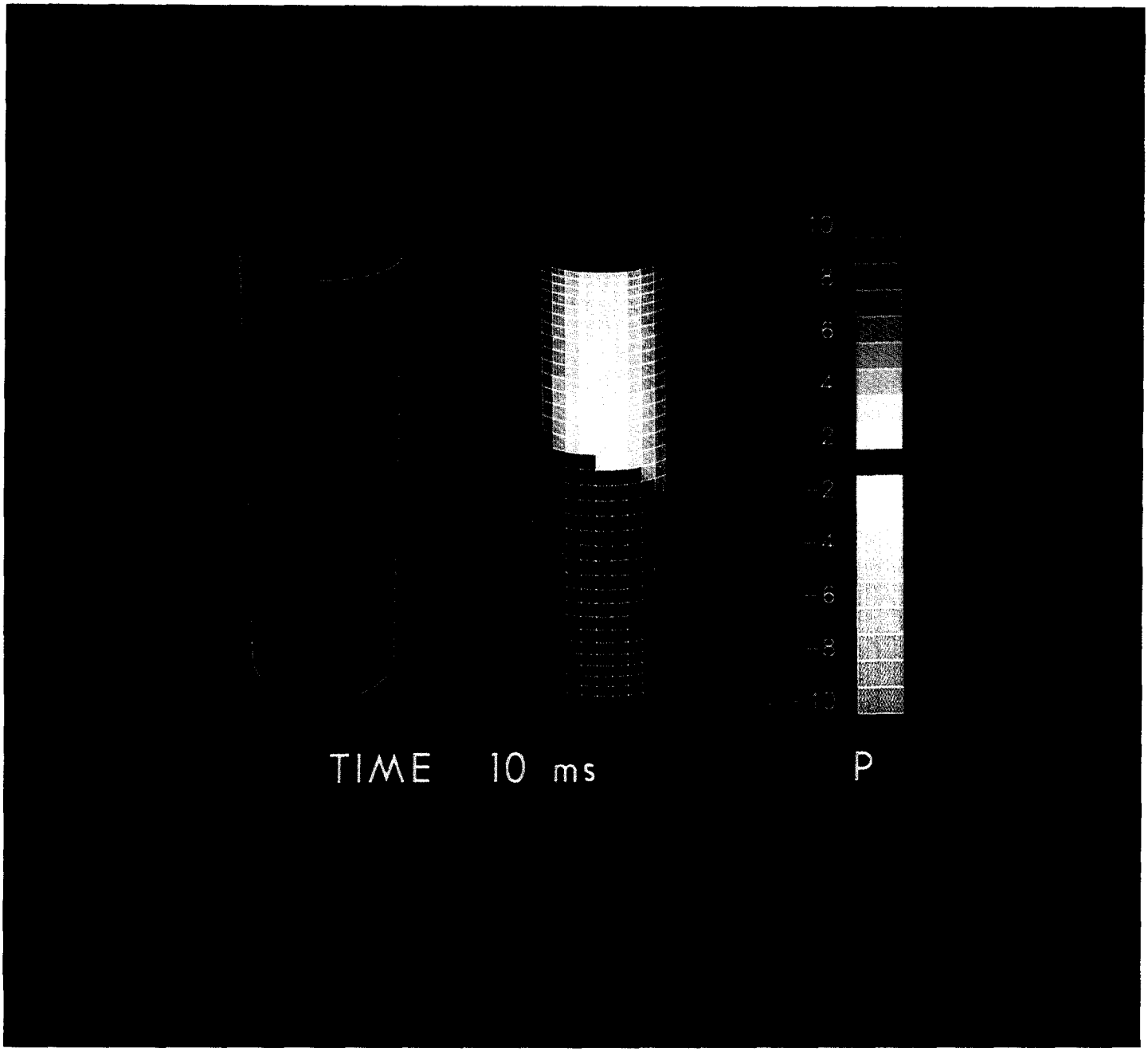

reactor components

by Anthony A. Amsden, Bart J. Daly, John K. Dienes, and John R. Travis

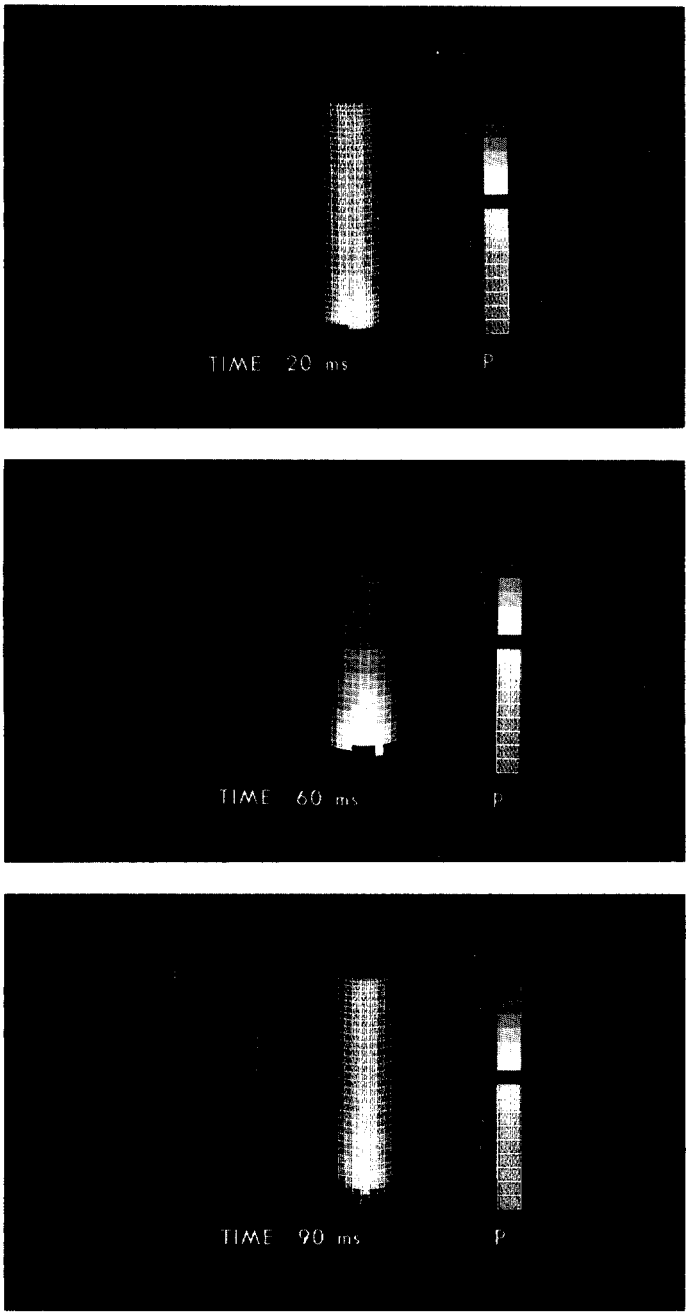

Detailed numerical modeling of multiphase flows for reactor safety analyses has a relatively short history. It began in 1974 with the development of the KACHINA code by Francis H. Harlow and Anthony A. Amsden of the Los Alamos Fluid Dynamics Group. KACHINA was the first code to provide stable numerical solutions for multidimensional two-phase fluid dynamics. Since that time. research efforts in reactor safety analysis based on this method have been established at many installations throughout the world. The Los Alamos effort has continued with the ongoing development of multiphase computational techniques and, more recently, with the application of these techniques to practical problems in reactor safety.

The numerical methods developed at Los Alamos formed the basis for TRAC, the large systems code that computes therma-hydraulic interactions throughout an entire reactor system during a simulated accident. The studies described here focus on separate effects-–flow and thermal interactions in particular components of a reactor. Separate-effects studies are usually performed in much greater detail than is possible with a systems code. Unlike TRAC. which computes approximate one-dimensional interactions in all components except the reactor vessel. separate-effects codes compute very detailed interactions in two and three dimensions and may include the dynamic interaction of fluids with structures.

Often, multidimensional studies reveal important phenomena that do not appear in one-dimensional studies, An example discussed in detail below is critical two-phase flow through areas of restricted flow, such as a nozzle or a small break in a pipe. Attempts to develop one-dimensional correlations to describe these flows were not very successful. A correlation that worked well for one type of nozzle could not produce accurate predictions for a different type. A two-dimensional study indicated that the problem arose from a failure to account for certain geometric variations in the nozzles. After geometric effects were included in the correlation, it was applied successfully to a wide variety of nozzle configurations and sizes. This improved correlation can now

be used with confidence in the systems codes.

The component codes do not generally employ empirical correlations for heat-transfer rates and other exchange functions. Instead, we develop thermal-hydraulic models from first principles and test their accuracy by comparing calculational results with experimental data. One notable example of such models is a set of constitutive relations for mass and momentum exchange in the mixing of steam and water by turbulent motion. These constitutive relations have been tested by extensive comparison with experimental data and then applied to practical reactor problems for which no experimental data are available.

Through this process of model development, comparison with experiment, and application to practical problems, we not only establish confidence in our own computational results, but we also demonstrate the capability of numerical methods for simulating complex multifluid and fluid-structure interactions. Our work has therefore helped to increase confidence in the results of analyses with large systems codes.

We will discuss in some detail our work on fluid-structure interactions and critical two-phase flow and describe briefly other efforts that illustrate the breadth of the modeling capabilities we have developed in this field.

Fluid-Structure Interactions

Pressurized-water reactors operate at relatively high pressure, typically about 150 bars (about 2250 pounds per square inch). Consequently, a sudden break of a large inlet or outlet pipe will produce strong depressurization waves that can create very high transient stresses in the reactor structure. Large-pipe breaks are not expected, even as a result of earthquakes, corrosion, or sudden changes in reactor power. However, reactor systems are designed so that, should one occur, the reactor itself would not be damaged and no significant amounts of radioactivity would be released. To determine the margins of safety under these extreme conditions, it is necessary to calculate in detail the dynamic interactions between the fluid and the structural components following a sudden break. Below we discuss interactions with two specific structures, the core barrel and the control-rod guide tubes (Fig. 1).

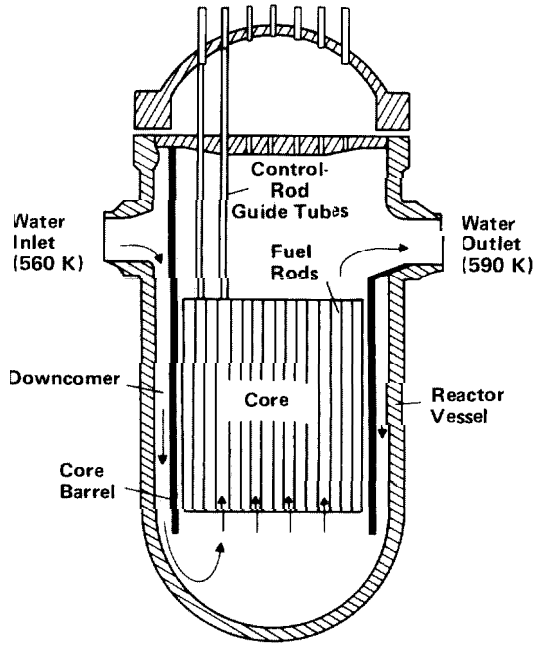

Fig. 1. Schematic diagram of the pressurized-water reactor components discussed in the text.

CORE BARREL RESPONSE TO INLET PIPE BREAK. A number of years ago, the Nuclear Research Center in Karlsruhe, West Germany (Kernforschungszentrum Karlsruhe) began a program to evaluate numerical models of fluid-structure interactions in reactors by comparing calculated results with experimental data. They were particularly interested in the response of the core barrel to a sudden, or guillotine, break in an inlet pipe. They made plans to perform experiments at Heissdampfreaktoranlage **(HDR),** an experimental facility near Frankfurt, West Germany, and, at the same time, asked a number of theoretical groups, including the Fluid Dynamics Group at Los Alamos, to predict the results of these experiments.

During normal operation, water enters the reactor vessel through an inlet pipe and flows down the downcomer and up through the core (see Fig. 1). The core is separated from the downcomer by a cylindrical steel shell, the core barrel. The core barrel serves a dual function: it holds the fuel rods rigidly in place and separates the cold incoming water from the hot water rising in the core.

Should an inlet pipe break, a depressurization, or rarefaction, wave will propagate into the downcomer at the speed of sound in the water, just under 1 meter per millisecond. As the wave propagates down the downcomer, it leaves a low-pressure region behind it. The resulting high pressure difference across the core barrel causes its outward displacement. In

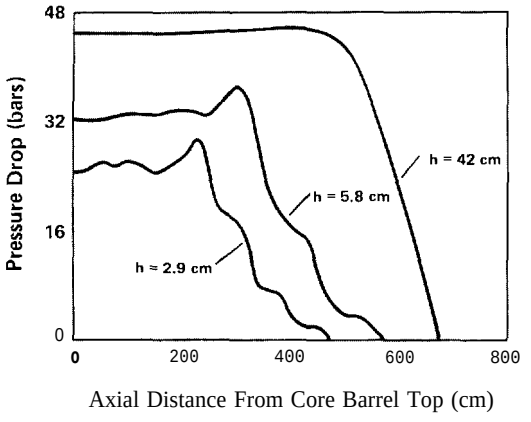

Fig. 2. Profiles of pressure drop in the downcomer showing the effect of wall thickness* h *on the wave structure of the rarefaction.

addition, a precursor wave propagates down the core barrel ahead of the main wave in the water (the speed of sound in steel is about 5 times greater than in water), but its effect is small. The motion of the core barrel generates acoustic waves in the water in the core, but their effect also is expected to be small.

These phenomena can be anticipated qualitatively, but five years ago when we undertook to quantify them, the available computer codes were inadequate to calculate the fluid pressure and the stresses in the core barrel. We needed three-dimensional codes for both the complex steam-water flow and the structural motion.

Los Alamos Calculations. To model the fluid motion we used K-FIX, a code for three-dimensional flow of two compressible phases. This code is based on the multifield technique of KACHINA and includes a fully implicit exchange of mass, momentum, and energy between the vapor and liquid phases. Phase transitions and interracial heat transfer are coupled to the fluid dynamics in the pressure iteration. The method reduces to the Implicit Continuous-fluid Eulerian (ICE) technique for single-phase flow.

To model the core barrel motion, we developed a special-purpose code called FLX that solves the Timoshenko shell equations with an explicit finite-difference technique. (In the earliest work on this problem, the core barrel motion was represented by the classical theory of beams, but we rejected this approximation because, for example, it cannot account for local deformations of the core barrel. particularly where the cylindrical shell bulges toward the break. We also rejected the normal-mode description chosen by the theoretical group at Kernforschungszentrum Karlsruhe because it is difficult to formulate mathematically and cannot easily accommodate changes in the boundary conditions or modification to the structure.) Our finite-difference version of the shell equations is relatively straightforward and can be integrated numerically with the very fine time and spatial resolution needed to simulate the complex wave patterns generated by sudden loading.

The coupling of fluid dynamics and structural motion is accomplished in two parts. The fluid-dynamics code computes the pressure gradient acting on the core barrel and this pressure gradient is used in the structural code that solves the Timoshenko shell equations, The motion of the core barrel changes the width of the downcomer and, through this volume change, affects the fluid density. The fluid-dynamics code then incorporates the new density and computes the corresponding flow and pressure fields.

It is not necessary to use the same zoning or time steps in the two codes. In fact, we usually run the structural code with a time step less than a tenth of that used in the fluid-dynamics code because of the relatively high sound speed in the steel core barrel.

To illustrate how the stiffness of the core barrel affects the propagation of the depressurization wave in the downcomer, we present in Fig. 2 some calculations performed with the coupled code. Shown are the pressure profiles in the downcomer at one point in time for three different thicknesses. A 42-centimeter-thick core barrel acts as if it were rigid. With a thickness of 5.8 centimeters (typical of reactor geometries), the elastic motion of the core barrel produces significant oscillations in the pressure profile. The oscillations increase in amplitude as the wall thickness is decreased further. The calculations show that the pressure drop behind the repressurization wave and the wave speed both increase with increasing stiffness of the core barrel. We have derived an approximate analytic expression for the average wave speed $\bar{c}$.

$$\bar{c} = \frac{c_0}{1 + (\rho c_0^2 a^2 / Ehb)} \quad , \tag{1}$$

where c_o is the speed of sound in the water, p is the density of the water, a and h are the radius and thickness, respectively, of the core barrel, b *is* the width of the downcomer, and E represents Young's modulus. This expression, like the calculation. shows the wave speed increasing with wall thickness,

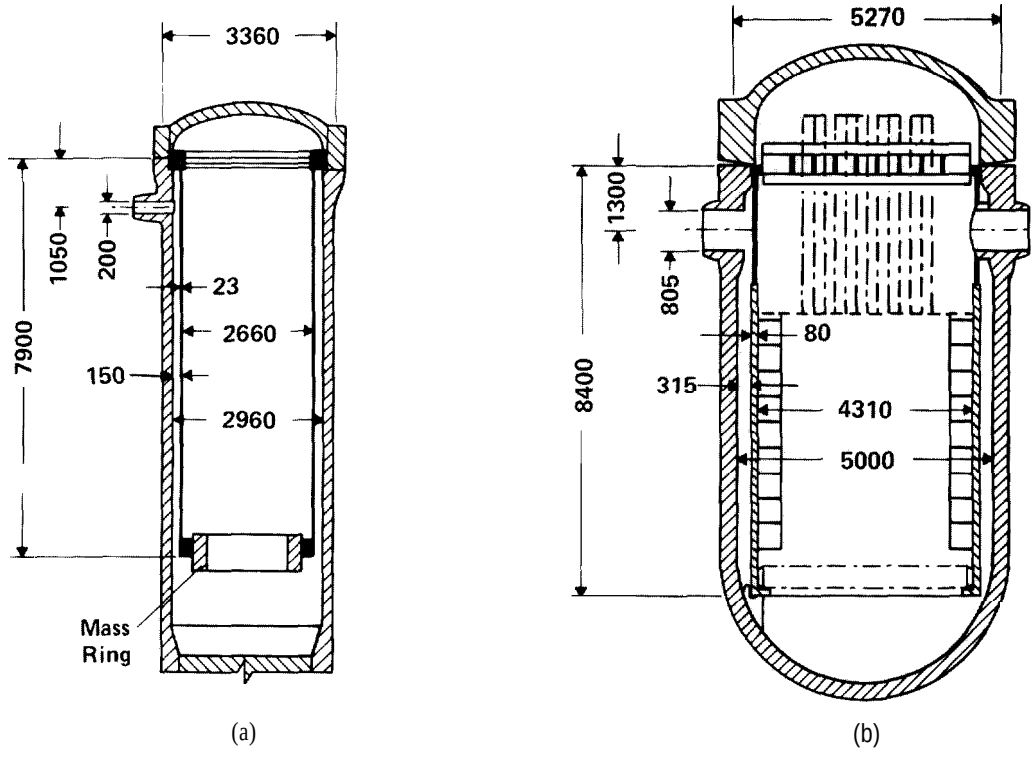

Fig. 3. Comparison of (a) HDR, the West German facility at which the depressurization experiments were performed, and (b) a typical pressurized-water reactor. The HDR mass ring simulates the mass of the fuel rods. Dimensions are in millimeters.

The HDR Experiment. In June 1980, the first of a series of experiments was carried out at HDR (Fig. 3). The fuel rods are simulated by a 10-metric-ton ring supported at the bottom of the core barrel. The height of the facility is typical of pressurized-water reactors, but its diameter is considerably smaller.

The response of the HDR core barrel to a guillotine break in a cold leg was monitored with about 75 instruments (pressure gauges, accelerometers, and strain gauges) that had been carefully selected and tested to operate at the temperature and pressure typical of a pressurized-water reactor. The initial temperature (540 kelvin) and pressure (108 bars) were supplied by electric heaters.

Before the experiment was carried out, six United States and West German groups calculated the response of the core barrel to a sudden break and submitted the pretest results to the Kernforschungszentrum Karlsruhe. The Los Alamos predictions for the pressure distribution and deflection of the core barrel at four times are shown in the opening figure. The core barrel undergoes transient oscillation but exhibits no per-

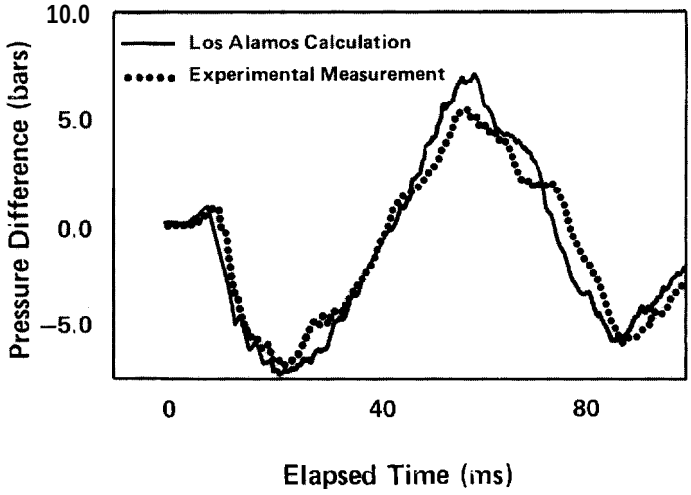

Fig. 4. Comparison of Los Alamos pretest prediction and HDR measurement of the pressure difference across the core barrel (at 330 cm below the inlet pipe) caused by a guillotine break in the inlet pipe.

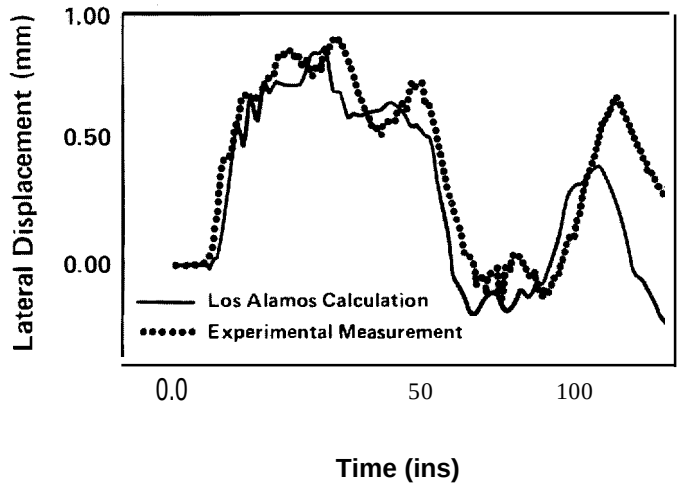

Fig. 5. Comparison of Los Alamos pretest prediction and HDR measurement of the displacement of the core barrel (at 330 cm below the inlet pipe) caused by a guillotine break in the inlet pipe.

manent deformation. Figures 4 and 5 show the good agreement between the Los Alamos calculations and the experimental data. This good agreement prompted a recent workshop on the HDR test to recommend that the Los Alamos coupled code be used for the official posttest calculation.

The good agreement between our calculations and the experiment is due in large part to the long lead time available to us. The coupled code evolved over a period of about five years, even though many of the techniques were already in hand at the beginning of the program. The level of accuracy finally achieved would not have been possible in a shorter time.

The structure and fluid flow in HDR are simplified compared to an operating reactor, but the comparison with experiment demonstrated that good predictions are possible. Commercial power reactors present many features in addition to those included in the HDR test, such as fuel rods, support plates, complex pipe breaks, and various flow restrictions. Accounting for these additional features will require a significant amount of additional work, but we feel that the capability for accurate calculations has been demonstrated.

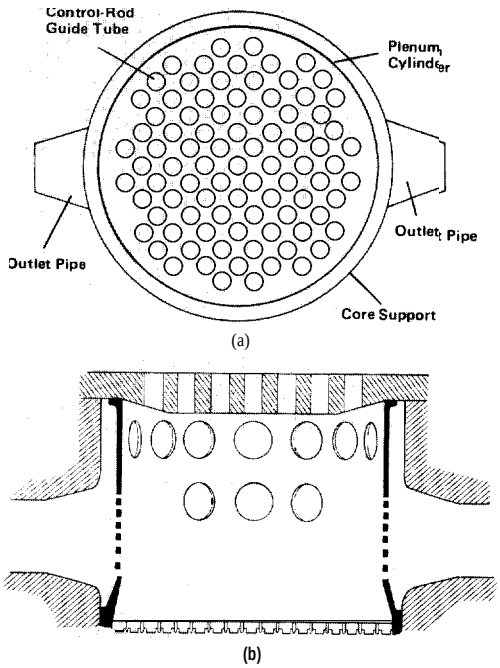

Fig. 6. Upper plenum of the pressurized-water reactor chosen for analysis of the effect of an outlet-pipe break on the displacement and possible deformation of the control-rod guide tubes. (We based our computer model on many of the features found in the West German Babcock-Brown Boveri reactor.) The top view (a) shows the location of the 89 control-rod guide tubes enclosed within the plenum cylinder, and the cross-sectional view (b) shows the large and small holes in the plenum cylinder through which water flows from the core to the outlet pipes. Fourteen large holes are distributed uniformly around the cylinder at a high level, and two diametrically opposite sets of three large holes are positioned at a lower level 90° from the outlet pipes. Two sets of 37 small holes are directly aligned with the outlet pipes. This hole arrangement, which forces much of the water to make a circuitous exit from the plenum to the gap between the plenum cylinder and the core support, @orals the guide tubes some protection from the effects of a rarefaction wave resulting from sudden depressurization in an outlet pipe.

CONTROL-ROD GUIDE TUBE RESPONSE TO OUTLET PIPE BREAK, Another fluid-structure interaction of importance is the effect of an outlet-pipe break on the control-rod guide tubes in the upper plenum of a pressurized-water reactor (see Fig. I). Would the guide tubes be deformed to such an extent that the control rods could not be lowered to shut down the reactor?

Analysis of this interaction involves the complex geometry of the upper plenum and the response of many guide tubes. The upper plenum of the reactor we analyzed (Fig. 6) included an arrangement of small and large holes in the plenum cylinder. This hole arrangement, which forces much of the flow to follow a circuitous path through the upper plenum, posed a particularly difficult modeling problem.

A three-dimensional fluid-dynamics code with considerable flexibility was required for the analysis. We chose SALE-3D, an implicit, three-dimensional, Arbitrary Lagrangian-Eulerian code that allows calculations in all flow-speed regimes. Written for the Cray computer, this code is particularly applicable to flows in highly complex geometries. It not only allows nonuniform zoning and curved boundaries, but, because it takes advantage of the high processing speed and large storage capacity of the Cray computer, it can also model geometric details with an accuracy never before practical. SALE-3D is used in tandem with a structural-response code that determines the guide-tube dynamics.

The fluid-dynamics computing mesh for the upper plenum (Fig. 7) is generated by distorting a Cartesian block of cells 52 across, 26 deep, and 10 high. The mesh approximates the circular cross section of each guide tube by 4 cells that form an octagon. The computing technique of SALE-3D permits the mesh to move with the fluid in a Lagrangian fashion, remain fixed in an Eulerian manner, or move in some arbitrarily specified way to provide a continuous rezoning capability.

Because early calculations had indicated that the elastic limit was likely to be exceeded for a number of the guide tubes, the goal of our analysis was an accurate assessment of the plastic response and resulting deformation. For this purpose, we subdivided each tube segment in the structural model into a set of 20 equal angular elements and used a sublayer model within each element to represent strain hardening. The structural-response code calculates the stresses, strains, deflections, and velocities in the horizontal plane for every segment of each guide tube, and also makes a record of those elements undergoing maximum stress and strain.

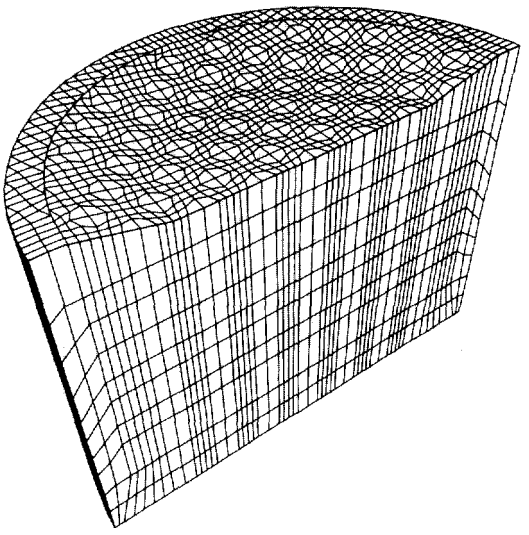

Fig. 7. Perspective view of the fluid-dynamics computing mesh for the upper plenum, which is created from a block of cells 52 cells wide, 26 cells deep, and 10 cells high. The front of the mesh lies on the symmetry plane that cuts through the midlines of the outlet pipes.

The transient calculation begins with a series of pressure changes at one of the two outlet pipes to simulate the depressurization resulting from a break. SALE-3D calculates the lateral forces on each guide tube at ten elevations, and these forces are then used to determine the guide-tube dynamics. The structural-response code returns the velocities for each elevation of each guide tube to SALE-3D. The guide-tube velocities are then applied as a boundary condition on the fluid flow, This interaction fully couples the fluid and structural dynamics. A plot of the velocity vectors in the fluid during depressurization is shown in Fig. 8. As a result of the fluid acceleration following depressurization, the transient speeds are nearly two and one-half times the steady-state values.

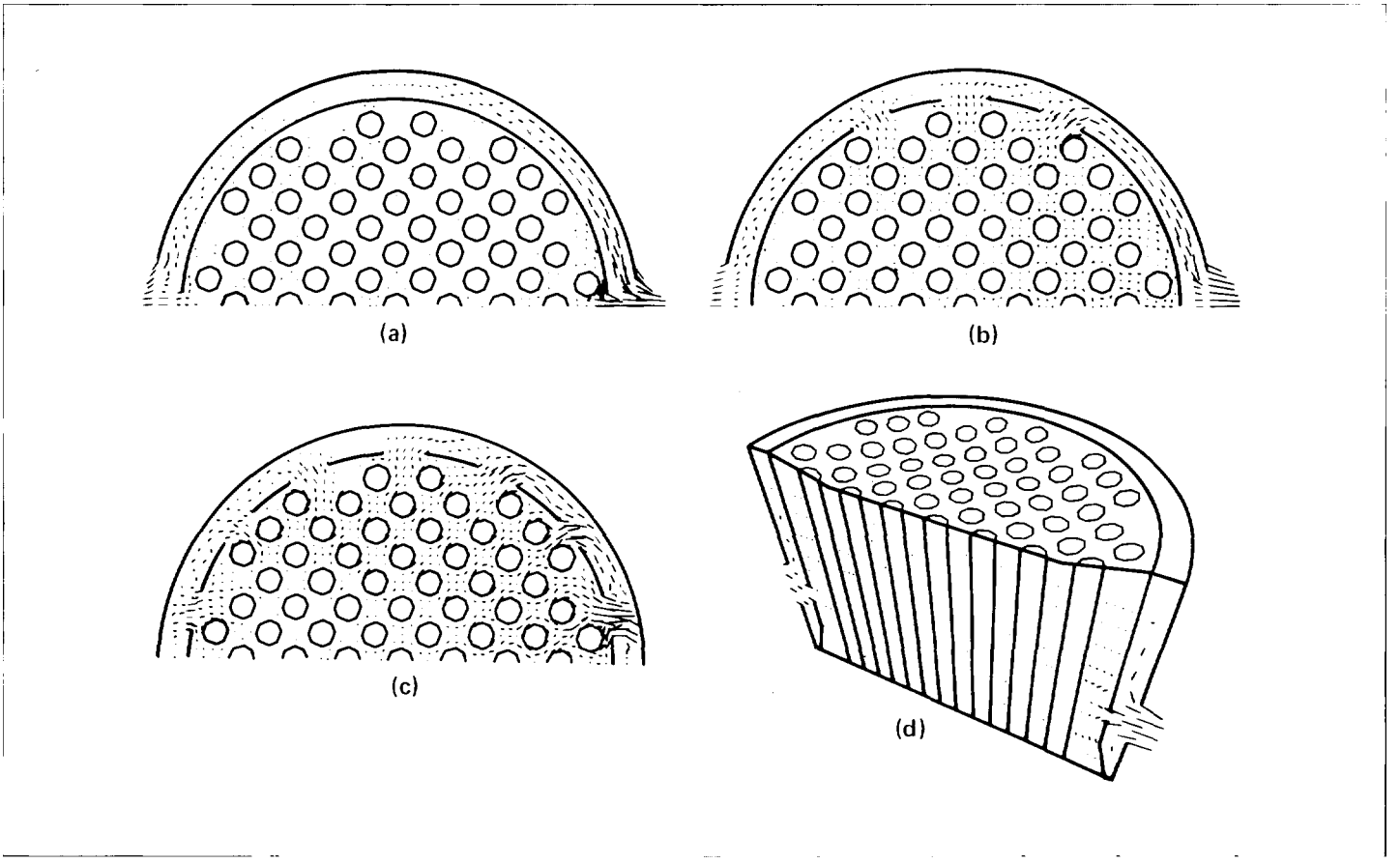

Fig. 8. Calculated velocity vectors showing the flow of water during a depressurization resulting from a break in the outlet pipe on the right. Shown are the vectors at (a) a horizontal level near the bottom of the outlet pipes, (b) at the horizontal level of the sets of three large holes in the plenum cylinder, (c) at the horizontal level of the sets of seven large holes in the plenum cylinder, and (d) across the vertical symmetry plane.

In this analysis, the water is assumed to persist in the liquid state throughout the early, most violent stages of depressurization, This assumption is based on the hypothesis that the initial pressure drop is the largest, and that it brings the fluid nearly to saturation, Subsequent pressure drops to levels low enough to initiate steam formation will be milder. Thus the greatest potential for damage occurs during the single-phase flow.

For damage assessment, it is the structural deformation that serves as the principal result from our analysis. The time histories of stresses and strains experienced by the guide tubes indicate that a break of an outlet pipe may cause significant plastic deformation in a number of the guide tubes.

These preliminary SALE-3D results demonstrate a new capability in modeling complex reactor flows. A more comprehensive program of study and comparisons with a variety of experimental data will be required to verify the code.

NEW CODES FOR FLUID-STRUCTURE CALCULATIONS. Other postulated breaks in a pressurized-water reactor can cause fluid-structure interactions. For example, a break in a steam generator would involve the barrier between the primary and secondary coolant circuits. Analysis of breaks in this structure is in a very primitive stage, but we anticipate that increasingly sophisticated methods will be developed to address such problems.

The analyses described above are carried out with general-purpose codes adapted to specific accidents. The ease of modifying these relatively simple codes permits the users to apply ingenuity and insight in solving particular problems. From a practical point of view, fluid-structure interactions are too complicated and too varied to be analyzed with a single general-purpose code. A more useful computational tool would be a family of versatile fluid and structural codes that can be coupled in various combinations, and indeed this is the direction in which investigators are moving.

Critical Flows in Two-Phase Systems

One of the most important phenomena determining the duration of the depressurization, or blowdown, phase of a large-break loss-of-coolant accident is the rate at which coolant exits from the broken pipe. We know from observation that the flow out the break reaches a maximum value independent of the pressure difference between the inside and the outside of the pipe break, provided that the pressure difference is greater than a critical value. This limiting flow phenomenon is called critical, or choked, flow. It is well understood for single-phase compressible fluids, but, at the time we began our study, thermodynamic models and one-dimensional fluid-dynamic calculations of two-phase critical flow often did not accurately predict the observed data. Calculated values of critical flow velocities were usually too large and had to be multiplied by empirically determined factors known as break-flow multipliers to achieve agreement with measured values. Our studies, based on a two-dimensional theory, show that nozzle geometry and non-equilibrium effects must be included to predict the critical flow velocity accurately.

When a single-phase compressible fluid flows through a nozzle, the critical flow velocity equals the speed of sound at the nozzle throat. The physical explanation is simple: When the fluid is moving with the speed of sound, a downstream pressure disturbance propagates upstream as fast as the fluid is moving downstream, so the net propagation of the disturbance is zero. Therefore, under critical flow conditions, the nozzle throat acts as a barrier to any downstream pressure changes. The limiting flow velocity can be altered only by changing the conditions upstream of the throat.

A vapor-liquid mixture, which is also a compressible fluid, exhibits a similar but much more complicated phenomenon. The critical flow velocity is still the sonic velocity at the throat, but the sonic velocity is affected by vaporization along the accelerating flow path, by the spatial distributions of the liquid and the vapor, and by nonequilibrium effects that occur when the liquid phase superheats because of rapid depressurization. The sonic velocity in a homogeneous two-phase mixture can be far less than the sonic velocity in either of the separate single-phase components. This reduction is attributed to the vapor's acting as a weak spring coupled to the large liquid masses.

TWO-DIMENSIONAL FLUID EQUATIONS. For the relatively high flow rates characteristic of critical flows, we assume a homogeneous modei for a steam-water mixture in which both phases move at equal velocities and are at the same temperature. (Because this temperature is not necessarily the saturation temperature of the mixture, the homogeneous model does not imply thermal equilibrium.) In a two-dimensional flow region of variable thickness, the equations governing the two-

phase mixture density ρ, the velocity components u and v, and the internal energy I are

$$\frac{\partial \rho}{\partial t} + \frac{1}{A}\left(\frac{\partial A \rho u}{\partial x} + \frac{\partial A \rho v}{\partial z}\right) = 0 \ , \tag{2}$$

$$\frac{\partial u}{\partial t} + u\frac{\partial u}{\partial x} + v\frac{\partial u}{\partial z} = -\frac{1}{\rho}\frac{\partial p}{\partial x} \ , \tag{3}$$

$$\frac{\partial v}{\partial t} + u\frac{\partial v}{\partial x} + v\frac{\partial v}{\partial z} = -\frac{1}{\rho}\frac{\partial p}{\partial z} \ , \tag{4}$$

and

$$\frac{\partial \rho I}{\partial t} + \frac{1}{A}\left(\frac{\partial A \rho I u}{\partial x} + \frac{\partial A \rho I v}{\partial z}\right) = -\frac{p}{A}\left(\frac{\partial A u}{\partial x} + \frac{\partial A v}{\partial z}\right) \ , \tag{5}$$

where p is the fluid pressure and ***A is*** the thickness of the flow region normal to x and z. These equations are derived from the three-dimensional equations by integrating the latter over the thickness ***A*** in the third direction and assuming negligible variation of all dependent variables in this direction. Effects of gravity and wall friction are neglected because of the high flow velocity and relatively short nozzle length.

To compute two-dimensional flow in cylindrical ***(r,z)*** geometry, the thickness A and the coordinate x are identified with the radial coordinate r. To compute one-dimensional axial flow in a variable area pipe, A is set proportional to the cross-sectional area of the pipe, u is held identically zero, and all x-derivatives are omitted from the equations, This latter situation arises automatically in the numerical solutions when the finite-difference mesh is defined to be only one cell wide in the x-direction.

Equations 2-5 must be supplemented by an equation for the macroscopic vapor density $\alpha\rho_v$, where ρ_v is the microscopic, or thermodynamic, vapor density:

$$\frac{\partial \alpha \rho_v}{\partial t} + \frac{1}{A}\left(\frac{\partial A \alpha \rho_v u}{\partial x} + \frac{\partial A \alpha \rho_v v}{\partial z}\right) = \Gamma \tag{6}$$

Here, Γ is the rate of production of vapor mass per unit volume.

The form of the phase-change model embodied in Γ is crucial if nonequilibrium effects are to be predicted correctly. Although we can only approximate the microphysical phenomena involved in vaporization, we have been able to develop a nonequilibrium phase-change model that works well for predicting critical flows. This model is discussed later.

EQUILIBRIUM TWO-DIMENSIONAL CALCULATIONS OF CRITICAL FLOW RATES. Using the homogeneous two-phase mixture model described above, we calculated the critical flow rate for a blowdown experiment at the Semiscale test facility. Semiscale is a small-scale version of a pressurized-water reactor primary system for studying loss-of-coolant accidents resulting from the break of a large cooling pipe. In the experiment that we analyzed the pipe break was simulated by a nozzle known as the Henry nozzle (Fig. 9). We used the conditions measured a short distance upstream from the nozzle

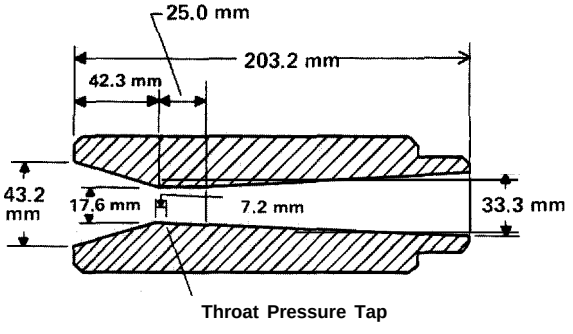

Fig. 9. Design of the Henry nozzle used at the Semiscale facility to simulate pipe breaks. Flow is from l@ to right.

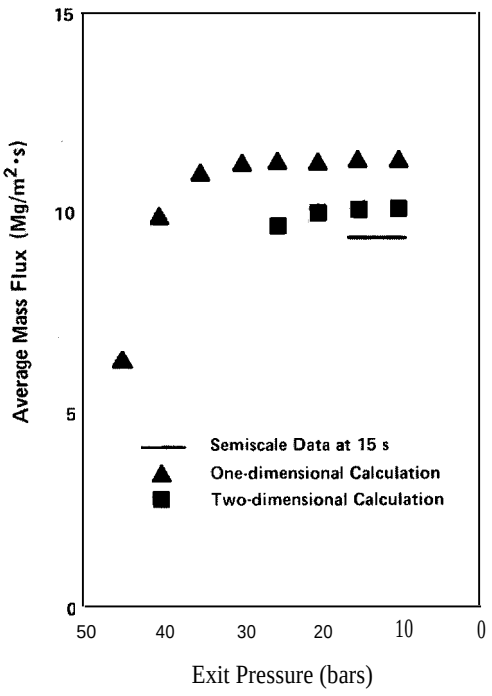

Fig. 10. Measured and calculated average mass fluxes as a function of nozzle exit pressure at 15 seconds into blowdown test S-02-4 at Semiscale.

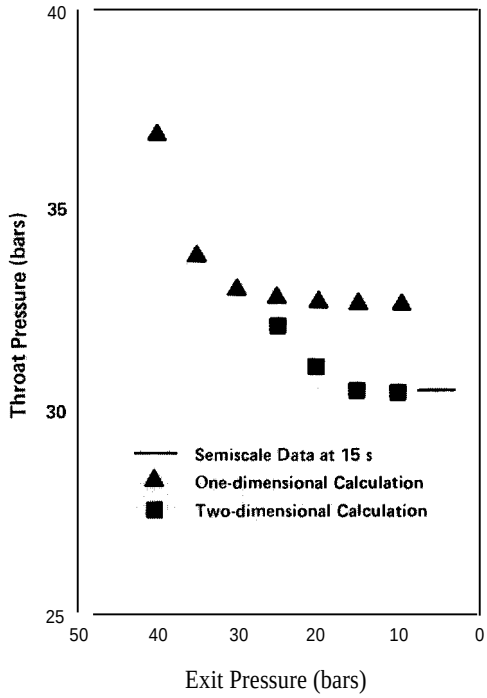

Fig. 11. Measured and calculated pressures at nozzle throat entrance as a function of nozzle exit pressure at 15 seconds into blowdown test S-02-4 at Semiscale.

entrance as boundary conditions for our calculations and solved the fluid equations in the immediate neighborhood of the nozzle.

Our initial calculations involved determining the critical flow rate 15 seconds after blowdown began. At 15 seconds, the vapor volume fraction is fairly large and the flow rate is likely to be independent of the vapor production rate, so we assumed an equilibrium phase-change model. In other words, Γ was chosen large enough to maintain the vapor and the liquid at the saturation temperature for each value of the local pressure. The boundary conditions upstream of the Henry nozzle entrance were 48 bars for the pressure, 534 kelvin for the temperature, and 56 kilograms per cubic meter for the mixture density.

We varied the pressure at the nozzle exit between 45 and 10 bars. For selected pressures in this interval, the computations were carried out until the flow reached a steady state, typically at 8 milliseconds after starting the flow from rest. The computed average mass flux and throat pressure are shown in Figs. 10 and 11. Figure 10 indicates that the flow reaches a limiting value as the exit pressure is reduced. The computed critical flow value is in good agreement with the measurements without the use of a break-flow multiplier or any other adjustment. The corresponding one-dimensional calculations also exhibit a critical flow as the exit pressure is reduced, but the computed mass flux must be multiplied by 0.833 to agree with the data.

To understand the nature of the two-dimensional effects, we

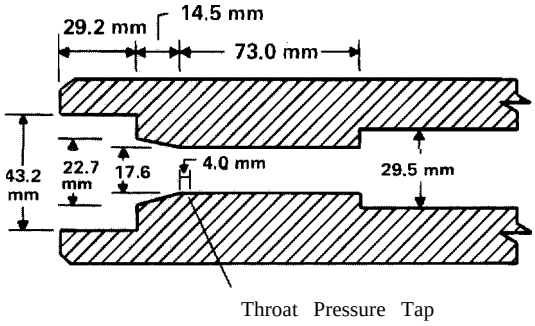

Fig. 12. Design of the nozzle normally used at the LOFT facility to simulate pipe breaks. The LOFT nozzle has a more abrupt throat entrance than does the Henry nozzle. Flow is from left to right.

carried out one- and two-dimensional calculations for a similar experiment in which the Henry nozzle was replaced by the nozzle design used at the **LOFT** (loss-of-fluid test) facility. Although the abrupt entrance to the throat of the **LOFT** nozzle (Fig. 12) would seem more likely to exhibit two-dimensional effects than the tapered entrance to the Henry nozzle throat, our one-dimensional results for the **LOFT** nozzle need only a small correction to agree with the two-dimensional calculation.

We studied the effect of entrance geometry further with a two-dimensional calculation for a Henry nozzle modified so that the entrance to the throat was abrupt rather than tapered. This change in geometry produced only a small change in the mass flow rate and the throat pressure.

Next we investigated the effect of varying the ratio of throat length to throat diameter for the general geometric configuration of the **LOFT** nozzle. Figure 13 shows the break-flow multipliers required to reach agreement between one- and two-dimensional calculations for various ratios. If the throat length is short relative to its diameter, two-dimensional effects are large. But for ratios greater than about 5, two-dimensional effects are no longer important and the exit flow can be described by a one-dimensional calculation.

A detailed look at the velocity profiles explains this effect.

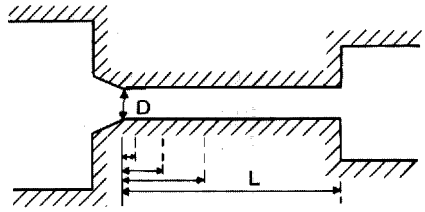

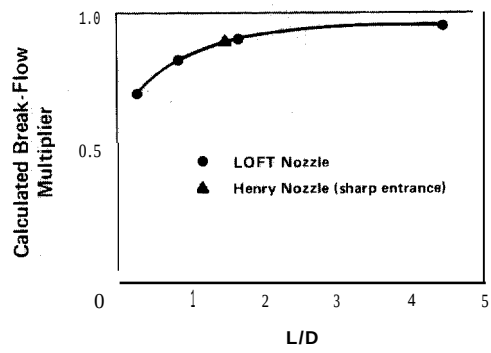

Fig. 13. Effect of the ratio of throat length L to throat diameter D on the calculated break-flow multiplier. Different L/D ratios for the LOFT nozzle were obtained by varying L as indicated.

At the throat entrance the radial velocity components are negative and, accordingly, accelerate the central axial velocities. Therefore, a strong radial velocity gradient develops in the entrance region. At a short distance downstream, the radial velocity components become positive and transfer momentum rapidly outward from the center. Here, approximate one-dimensional velocity distributions develop. However, if the throat length is too short for the flow to develop a one-dimensional velocity profile, the one-dimensional models will require a break-flow multiplier to agree with observed data.

EFFECTS OF NONEQUILIBRIUM PHASE CHANGE. The calculations presented so far have corresponded to homogeneous equilibrium phase change. To assess the relative importance of nonequilibrium phase change, we calculated the mass flow rates at the nozzle exit during the first 20 seconds of blowdown using two phase-change models, the equilibrium model described above and a model in which the phase change is zero. Figure 14 shows the calculated values and experimental data for the Henry nozzle. The values were obtained by multiplying the results of a one-dimensional calculation by the calculated break-flow multiplier for the Henry nozzle.

During the first 3 seconds of blowdown the fluid entering the nozzle is single-phase liquid. Its temperature is initially 28 kelvin below the saturation temperature, but, as the pressure decreases, the fluid rapidly reaches the saturation point and becomes superheated, The fact that the data lie between the calculated extremes indicates that nonequilibrium phase change occurs during these first few seconds.

After 3 seconds, when a two-phase mixture enters the nozzle, the calculation with equilibrium phase change agrees with the data. Finally, after 10 seconds when the mixture entering the nozzle is mostly steam, the calculated mass flow rates for both vaporization models coincide with each other and agree with the data. The flow rate is independent of the vapor production rate and is solely determined by the upstream conditions.

To calculate the nonequilibrium effects during the first 3 seconds, we need a detailed model of nonequilibrium vaporization. In a stationary environment, depressurization would lead to vapor production and bubble growth with the growth rate controlled by heat conduction to the bubble surface according to the relation

$$\frac{dr}{dt} = \left(\frac{6}{\pi}\right)\left(\frac{1}{r}\right)\left(\frac{\rho_l}{\rho_v}\right)^2 \alpha_l \left[\frac{C_l (T_l - T_{\text{sat}})}{L}\right]^2 , \qquad (7)$$

where r is the bubble radius, ρ_l is the microscopic liquid density, a_l is the liquid thermal diffusivity, C_l is the liquid specific heat, T_l is the bulk liquid temperature, T_{sat} is the saturation temperature, and L is the heat of vaporization. During the depressurization and acceleration of the fluid through a converging nozzle, the bubble growth rate varies because T_{sat} and ρ_l, depend on the pressure and T_l decreases as heat is used to vaporize the liquid. The instantaneous bubble radius thus depends on the entire bubble history.

The vapor volume fraction a is related to r and N, the number of bubbles per unit of mixture, by

$$\alpha = N\left(\frac{4}{3}\pi r^3\right) . \qquad (8)$$

Combining Eqs. 7 and 8 we derive the following expression for Γ.

$$\Gamma = \rho_v \frac{\partial \alpha}{\partial t} = \rho_l \left(\frac{18}{\pi}\right)\left(\frac{\alpha}{r^2}\right)\left(\frac{\rho_l}{\rho_v}\right)\alpha_l \left[\frac{C_l (T_l - T_{\text{sat}})}{L}\right]^2 . \qquad (9)$$

For application to the highly dynamic environment of a critical flow, we retain the form of Eq. 9 but choose a liquid thermal diffusivity and bubble radius that reflect the combined

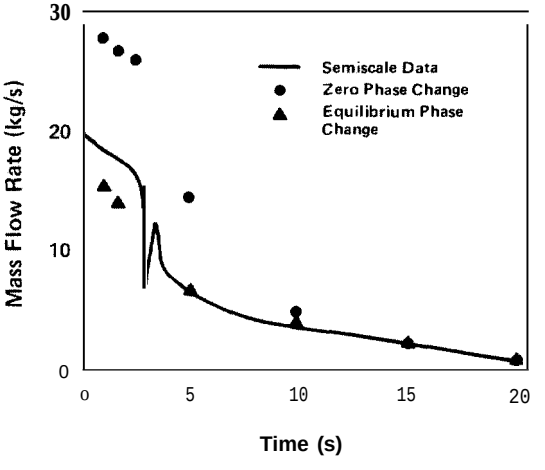

Fig. 14. ***Measured and calculated mass flow rates during the first 20 seconds of blowdown test S-02-4 at Semiscale. The calculations are based on two phase-change models, an equilibrium model and a model in which the phase change is zero.***

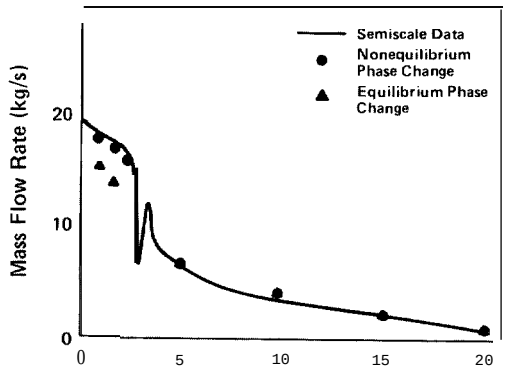

Fig. 15. Measured and calculated mass flow rates during the first 20 seconds of blowdown test S-02-4. The calculations are based on nonequilibrium and equilibrium phase-change models.

effects of relative motion and turbulence. These modifications allow the model to approach the correct limit in a quiescent environment.

In general, there is a spectrum of bubble radii, but we choose the critical radius for bubble breakup to characterize this spectrum. We determine an initial bubble radius by specifying initial values of N and a. The bubbles grow according to Eq. 7 with a_l replaced by a, a liquid thermal diffusivity enhanced by relative motion and turbulence. Consequently, the bubbles grow faster than the conduction-controlled rate. The bubbles continue to grow until they reach a critical size, determined by a Weber number criterion, and then begin to break up. The Weber number characterizes the competition between the dynamic forces that lead to bubble breakup and the restoring force of surface tension. From this point on, the typical bubble radius is taken as the critical radius and the specified initial number of bubbles no longer plays a role.

The critical radius for bubble breakup is given by

$$r_{\text{critical}} = \frac{2.3\sigma}{\bar{v}^2 \, (\rho_l^{\,2} \, \rho_v)^{1/3}} , \qquad (10)$$

where σ is the surface tension and $\bar{v}$ is the relative speed between the bubble and the surrounding fluid. To include the contribution of local turbulent fluctuations in the liquid to the relative speed we write $\bar{v}$ as

$$\bar{v} = \beta v_l \quad , \qquad (11)$$

where v_l is the liquid speed and β is a function of vapor fraction. We choose values of β consistent with observed turbulent velocity fluctuations, which are generally less than 10 per cent of the mean flow velocity. Toward the middle vapor-fraction range, β increases because of increased turbulent mixing from the higher shear flow associated with thinning liquid sheets. The increase in β may also result from an increase in mean relative velocity.

The enhanced liquid thermal diffusivity $\bar{\alpha}$ that replaces α_l in Eq. 9 is

$$\bar{\alpha} = \alpha_l + Br\bar{v} \ , \qquad (12)$$

where ***B is*** an empirically determined dimensionless constant. The value of ***B = 0.1*** matches the flow rate data for the Semiscale tests. The range of applicability of this value can only be accurately established after extensive data comparisons.

In Fig. 15, the nonequilibrium results for the mass flow rate during blowdown are compared with the data for the Henry nozzle from Fig. 14. The nonequilibrium results agree very well with the measured mass flow rate during the entire period of blowdown. However, at early times the calculated throat pressures (Fig. 16) are higher than the measured wall pressures at the throat entrance. This difference is probably caused by a rarefaction region in the proximity of the comer that is not modeled by the one-dimensional calculation,

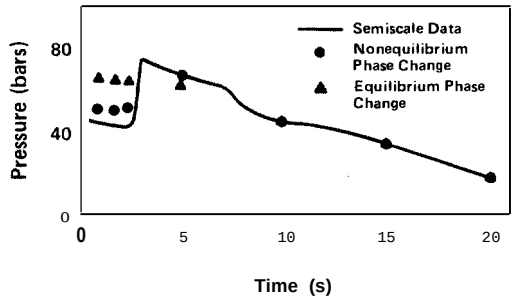

Fig. 16 Measured and calculated pressures at entrance to nozzle throat during the first 20 seconds of blowdown test S-02-4 at Semiscale. The calculations are based on nonequilibrium and equilibrium phase-change models.

In addition to these small-scale tests, the nonequilibrium model has been tested against data obtained from the full-scale critical flow project at the Marviken facility in Sweden, from the low-pressure **MOBY DICK** loop at the Nuclear Studies Center in Grenoble, France, and from the low-pressure critical flow loop at Brookhaven National Laboratory, These tests involved fluid pressures from about 90 bars down to slightly greater than 1 bar. Pipe diameters ranged from 75 centimeters down to a few centimeters. We encountered no scaling problems in going from small- to full-scale geometries because the nonequilibrium model is based on local flow and thermodynamic conditions.

This study has proved to be an important contribution in predicting two-phase homogeneous critical flows through

SUPPRESSION-POOL DYNAMICS IN BOILING WATER REACTORS

The suppression pool of a boiling-water reactor system is designed to condense steam that might fill the containment building following the break of a coolant pipe. The vents leading into the pool must be cleared of air before the steam can enter the pool. To study this process, we used a small-scale model consisting of a cylindrical container with a single axisymmetric vent entering into the water pool. The hydrodynamic phenomena associated with vent clearing were simulated with the SOLA-VOF code. Typical computed free-surface configurations and velocity vector fields are shown. Water velocities are indicated in blue, the water/gas interface in green, and the gas as black voids. The final figure in the sequence shows the high-pressure gas from the vent about to break through the water surface.

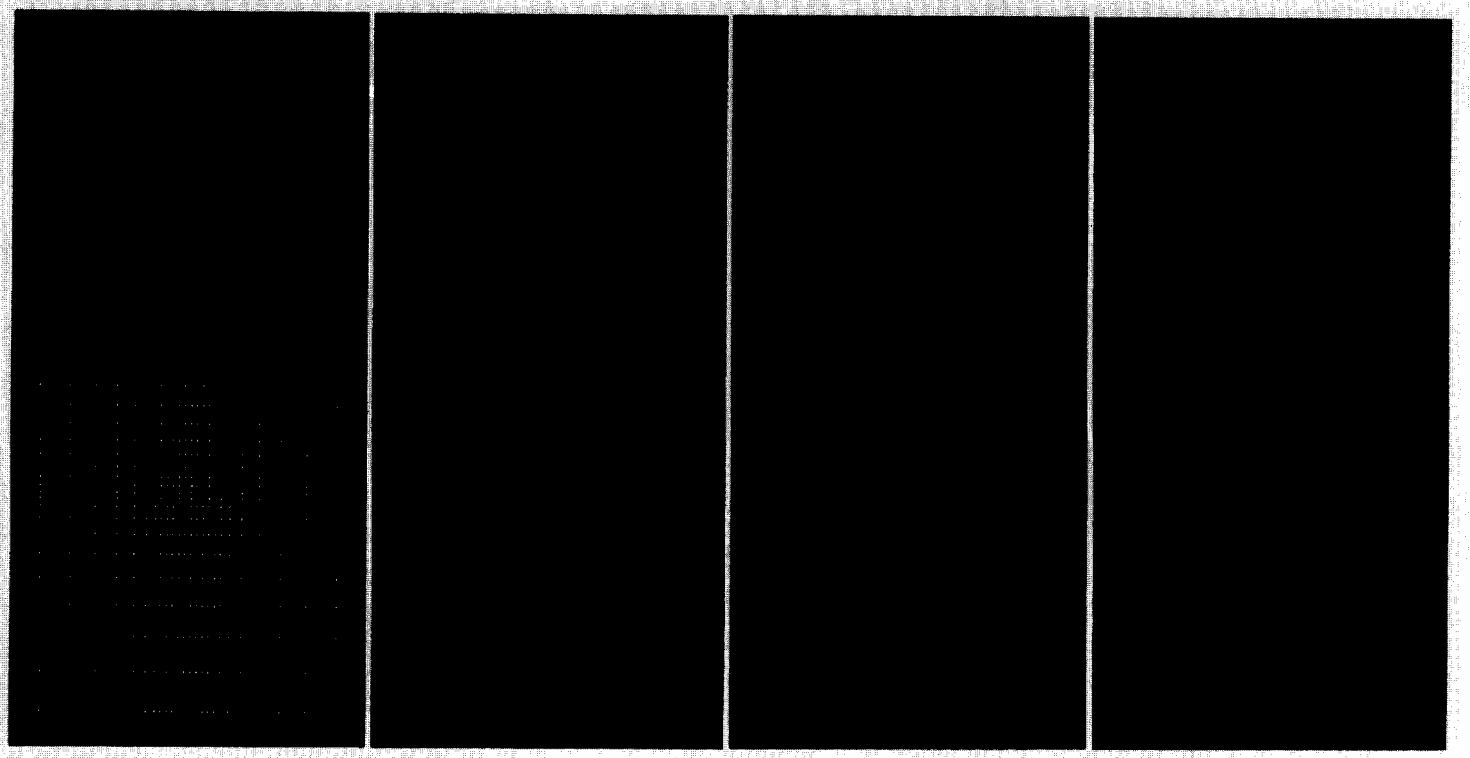

nozzles. We have shown that two-dimensional geometric effects not accounted for in one-dimensional calculations reduce the critical flow rates and therefore extend the duration of blowdown. We have also shown that nonequilibrium effects reduce the duration of blowdown because they increase the sound speed and therefore the critical flow rates.

The problems discussed above are only a small sampling of the component studies carried out in the Fluid Dynamics Group. To illustrate the broad applicability of the numerical techniques developed for reactor safety, four other studies are described briefly in the accompanying illustrations. One concerns liquid-metal fast breeder reactors, and the others deal with pressurized-water reactors. ■

THE WATER-HAMMER EFFECT

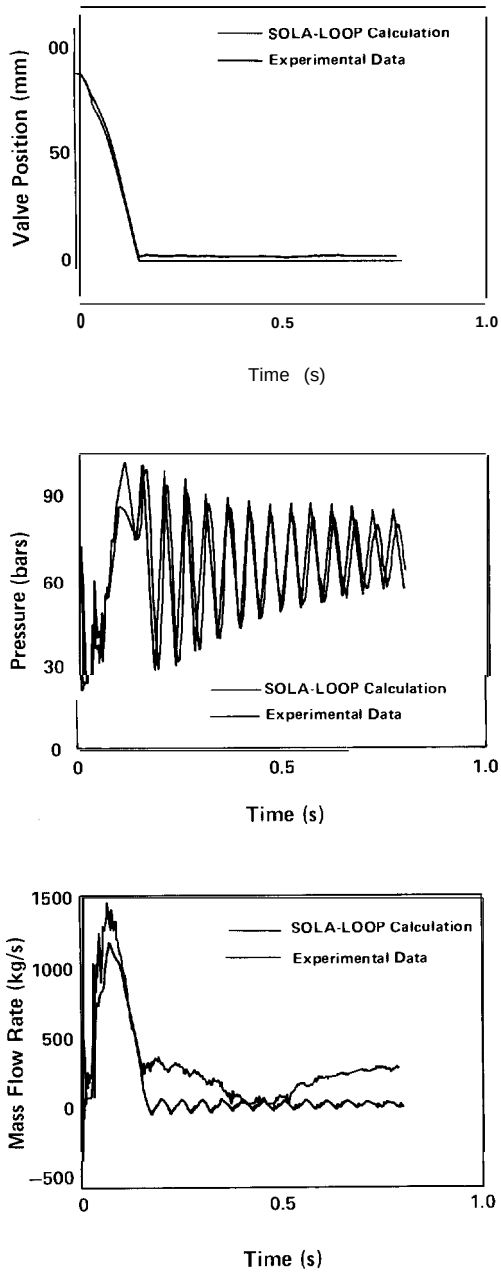

A few commercial pressurized-water reactors are equipped with valves in each primary loop that close automatically and rapidly if a break should occur in the loop. The function of these loop isolation valves is to limit the loss of coolant and, hence, the escape of radioactive materials to the containment building.

The rapid closing of the valves can, however, produce large pressure oscillations within the pipe, the so-called water-hammer effect. The forces produced by the break itself (pressure-release waves) and by the water-hammer effect can lead to considerable stresses on the valve, pipe, and supports.

We calculated the flow in the pipe network of the West German Speisewasserrückschlagventils (SRV) 350 blowdown experiments with SOLA-LOOP, a nonequilibrium, drift-flux code for calculating two-phase flow in pipe networks. The model for the dynamic behavior of the valve is given by $m(d^2x/dt^2) = \sum F$, *where* x *is the valve position and the forces* F *are the viscous drag, the pressure force, the damping force, the external actuating force and/or spring force, and the gravitational force. SOLA-LOOP supplies time-dependent fluid velocities, densities, and pressures to the valve model, and in return, the valve model calculates a time-dependent valve position that is used to determine the resistance to flow through the valve.*

Shown here are measured and calculated time histories for the valve position (top), the pressure just upstream of the valve (middle), and the mass flow rate just upstream of the valve (bottom). The changes in slope of the valve position curve at 75 millimeters (0.03 second) and at 45 millimeters (0.1 second) correspond to pressure spikes during the valve-closing portion of the experiment (≤0.15 second). After the valve closes, the water-hammer effect (1/4 period pressure waves) are set up in the isolated pipe between the closed valve and the reactor vessel. These waves decay in time, but their large amplitude may create damaging stresses in certain structural components. The mass flow rate increases as the blowdown commences and then decreases as the closing valve creates flow resistance. Although the measured valve position indicates that the valve is closed, the measured mass flow-rate data indicate some leakage through the valve between 0.15 and 0.4 second and a rebounding of the valve head at approximately 0.5 second.

CORE-BUBBLE DYNAMICS FOR BREEDER REACTOR ACCIDENT ANALYSIS

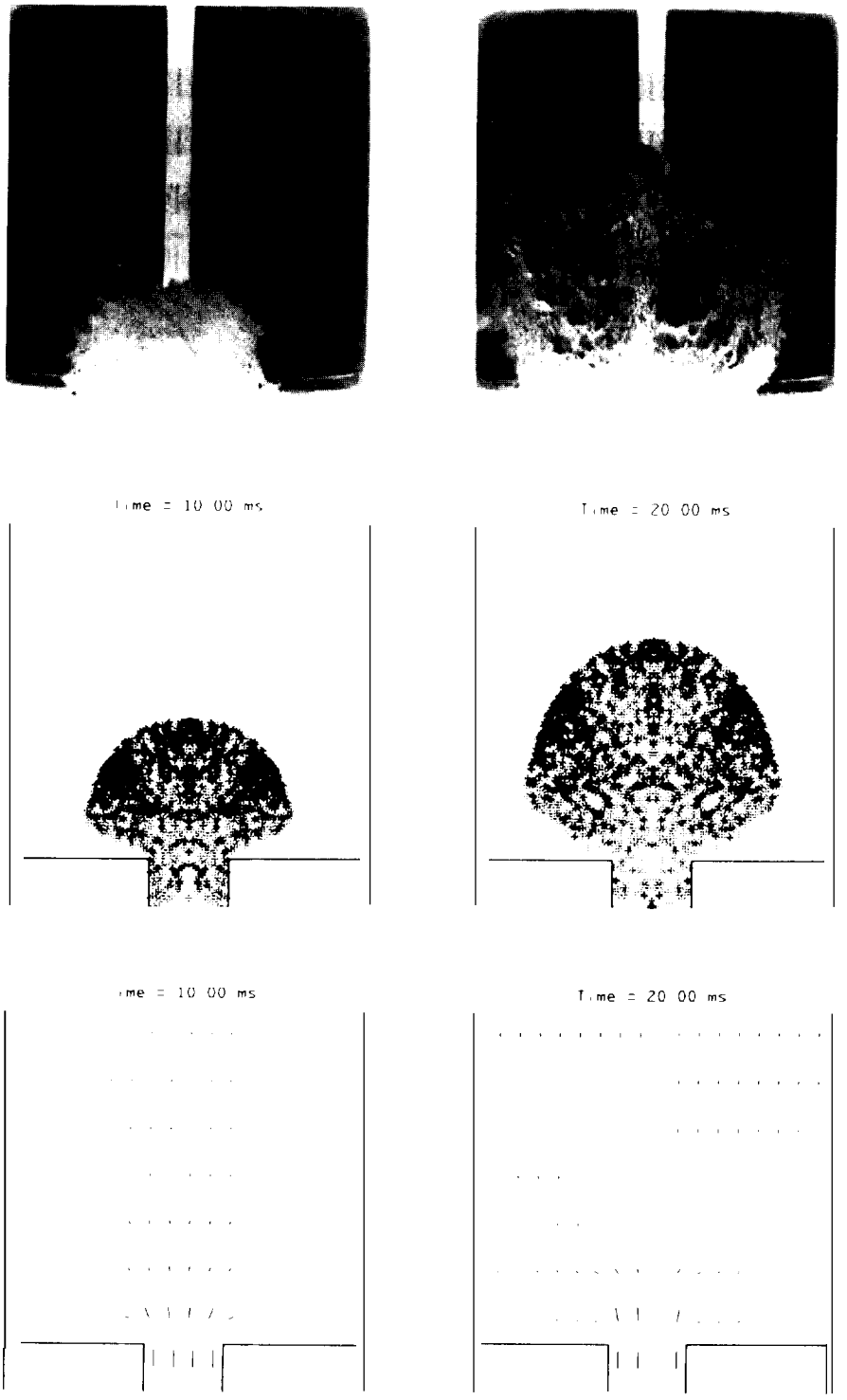

Safety analysis of the liquid-metal fast breeder reactor currently focuses on hypothetical core-disruptive accidents. In one hypothetical scenario, a sudden increase in fuel temperature due to a power burst causes the fuel to melt and vaporize at very high pressures. The expanding bubble of fuel vapor can then vent through the upper core structure into the sodium pool that covers the core region.

The dynamics and energy yield of this bubble ejection must be determined before we can assess the mechanical work that would be done by the sodium pool on the vessel head. The dynamics of the bubble expansion have been simulated by experiments in which a chamber filled with high-pressure air is ruptured and the resulting high-pressure jet of air expands into a water-filled chamber above. Shown here are frames (courtesy of Argonne National Laboratory) from a high-speed motion picture of one experiment and corresponding plots of marker particle configuration and velocity vector field calculated at Los Alamos.

As a diaphragm to the high-pressure chamber is ruptured, the surge of air increases the pressure in the water-filled

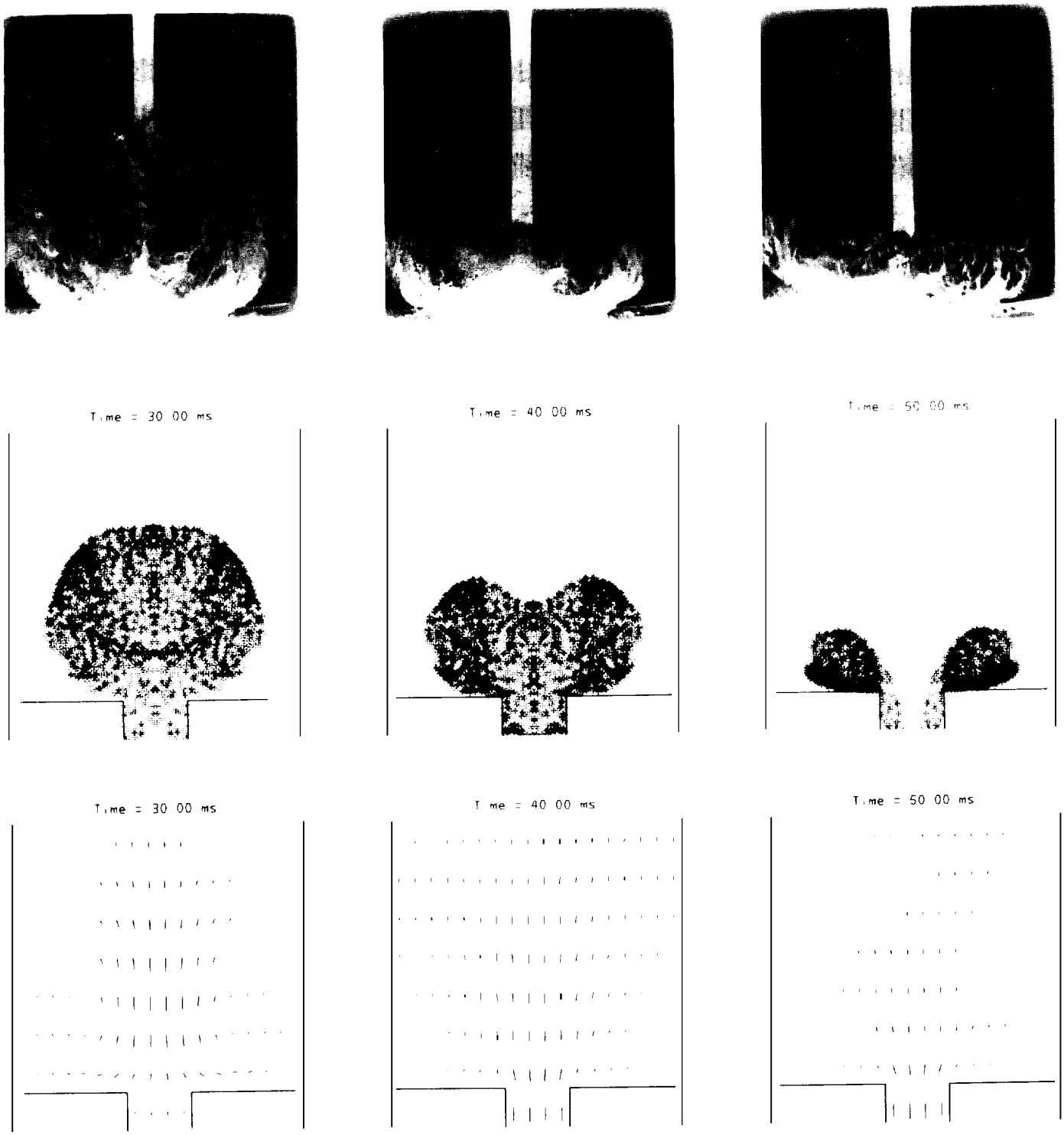

chamber. The momentum imparted to the water leads to an overexpansion of the air arid a subsequent drop in" bubble pressure. The pressure continues to decrease until 28 milliseconds when the bubble reaches its maximum volume. The bubble begins to collapse into the toroidal shape shown at 40 and 50 milliseconds. During the collapse the bubble pressure increases from the downward-directed momentum of the water. Beyond 50 milliseconds the pressure tends to equilibrate, and the bubble breaks up under the action of turbulence and buoyancy.

The velocity vector field shows a spherical distribution at 10 and 20 milliseconds. At later times, the bubble collapse is evidenced clearly by the reversal of the velocity vectors and the secondary-flow vortex pattern set up between the centerline and outside boundary. The vortex becomes smaller untill at 50 milliseconds it is isolated in a corner with most of the velocity vectors directed toward the lower chamber opening.

STEAM-WATER JET IMPINGEMENT ON REACTOR STRUCTURES

Other Studies

Nuclear power plant structures and components must be designed to withstand the impingement of a steam-water jet released from a hypothetical broken coolant pipe. We performed a two-phase calculation in cylindrical symmetry to simulate this interaction. Shown here are the velocity vector plot (top) and pressure field plot (bottom) for a high-pressure jet of hot water issuing from a break and impinging on a safety baffle. The velocity vector plot shows that the flow accelerates as it leaves the pipe, The acceleration is caused by flashing of the water to steam as the pressure drops below saturation pressure. The pressure contours show the pressure dropping rapidly as the flow exits from the pipe and then rising sharply near the center of the baffle. Proper design of safety baffles and pipe restraints requires accurate computation of this pressure field.

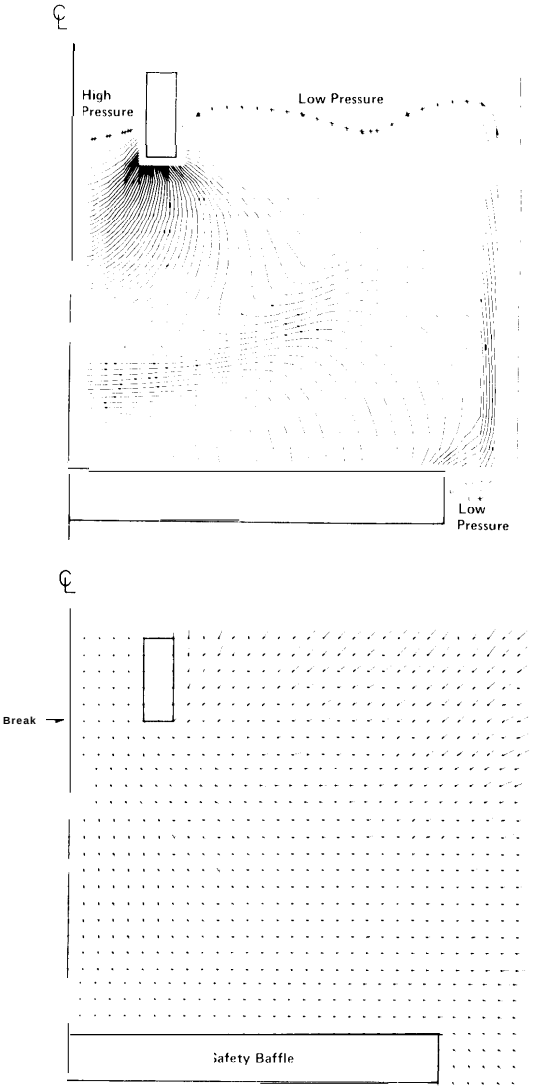

Further Reading

W. C. Rivard and M. D. Torrey, "K-FIX: A Computer Program for Transient, Two-Dimensional, Two-Fluid Flow," Los Alamos Scientific Laboratory report LA-NUREG-6623 (April 1977) and three supplements.

J. R. Travis, C. W. Hirt, and W. C. Rivard, "Multidimensional Effects in Critical Two-Phase Flow," Nuclear Science and Engineering, 68,338 (1978).

C. W. Hirt, N. C. Romero, M. D. Torrey, and J. R. Travis, "SOLA-DF: A Solution Algorithm for Nonequilibrium Two-Phase Flow," Los Alamos Scientific Laboratory report LA-7725-MS (June 1979).

J. K. Dienes, C. W. Hirt, W. C. Rivard, L. R. Stein, and M. D. Torrey, "FLX: A Shell Code for Coupled Fluid-Structure Analysis of Core Barrel Dynamics," Los Alamos Scientific Laboratory report LA-7927 (November 1979).

W. C. Rivard and J. R. Travis, "A Nonequilibrium Vapor Production Model for Critical Flow," Nuclear Science and Engineering 74,40 (1980).

C. W. Hirt and B. D. Nichols, "Volume of Fluid (VOF) Method for the Dynamics of Free Boundaries," Journal of Computational Physics 39, 201-225 (January 1981).

A. A. Amsden, J. K. Dienes, F. H. Harlow, and H. M. Ruppel, "Three-Dimensional Analysis of Fluid-Structure Interactions During Blowdown of an Upper Plenum," Los Alamos National Laboratory report LA-8754-MS (March 1981).

A. A. Amsden and H. M. Ruppel, "SALE-3D: A Simplified ALE Computer Program for Calculating Three-Dimensional Fluid Flow," Los Alamos National Laboratory report LA-8905 (in press).

W. C. Rivard, M. D. Torrey, and C. W. Hirt, "Post Test Evaluation of K-FIX Computations for a HDR Blowdown Test," Second International Seminar on Fluid-Structure Interaction and Internal Loading in Thermal Reactors, Ispra, Italy, August 24-25, 1981. (To appear in a special issue of Nuclear Engineering and Design.)

B. A. Kashiwa, R. B. Demuth, F. H. Harlow, and H. M. Ruppel, "Pre-Test Analysis of HDR Jet Impingement Tests V67.1 and V67.2," Los Alamos National Laboratory report (in preparation).

Acknowledgment

Other members of the Fluid Dynamics Group have played major roles in the studies described here. The authors would particularly like to acknowledge the contributions of Ronald N. Griego, Francis H. Harlow, Cyril W. Hirt, Bryan A. Kashiwa, Billy D. Nichols, William C. Rivard, Hans M. Ruppel, Leland R. Stein, and Martin D. Torrey.

AUTHORS

Anthony A. Amsden specializes in the application of high-speed computers to the numerical solution of complex problems in fluid dynamics. His particular interests are developing computer logic, programming large-scale multidimensional codes, analyzing calculations, and writing comprehensive reports and papers so that others can apply his work to their own investigations. Amsden's experience in computing at Los Alamos extends over twenty years, when he began as a systems programmer for the IBM-7030 (Stretch) computer. Afterward, he moved into scientific programming, where he has participated in developing many well-known computing methods, such as PIC for high-speed flow applications, IMF for multi-fluid flows, and the ICED-ALE and SALE families of programs. At Los Alamos, these programs have had direct application to reactor safety and weapons. The same programs are in use in private industry and scientific research installations throughout the world. Currently, he is developing a three-dimensional program for internal-combustion engine studies.

Bart J. Daly earned his Bachelor of Arts in geology and mathematics from the University of Wyoming in 1950 and his Master of Arts in mathematics from Arizona State University in 1960. In the intervening years he worked in the field of geophysical oil exploration. He has been in the Fluid Dynamics Group since joining the Laboratory in 1960. He has developed and applied numerical methods for fluid-dynamics studies, particularly in the areas of hydrodynamic instability, turbulence modeling, multifluid exchange processes, and reactor safety research. Currently, he is the Fluid Dynamics Group's project leader for Nuclear Regulatory Commission programs.

John K. Dienes received a Bachelor of Arts in mathematics from Pomona College and a Ph.D. in applied mechanics from the California Institute of Technology, where he was a Gillette Fellow. He worked in the aerospace industry on aeroelastic and control problems until 1963, when he joined General Atomic Company to participate in the Orion Program, a system for interplanetary nuclear-pulse propulsion. There he became acquainted with the fluid-dynamics codes developed at Los Alamos. Since joining the Laboratory's Fluid Dynamics Group in 1975, he has been interested in the application of these codes to a variety of problems, including fluid-structure and fuel-coolant interactions in nuclear reactors. He has also been involved with impact and explosive cratering, particularly in the development of constitutive laws for the deformation and fragmentation of solids at extreme pressures and strains, and has published over a hundred articles and reports in this field.

John R. Travis earned his Bachelor of Science with honors from the University of Wyoming in 1965 and received his Ph.D. from Purdue University in 1971. During his graduate studies, he was the recipient of an Advanced Studies Program Fellowship at the National Center for Atmospheric Research in Boulder, Colorado, where he conducted the research for his doctoral dissertation in computational fluid dynamics. From 1971 to 1973 he was with Argonne National Laboratory, where he was involved in the development of the fast reactor safety analysis code SAS. He joined the Laboratory's Chemistry-Materials Science Division as a Staff Member in 1973, where he developed a numerical model for predicting the redistribution within the atmospheric boundary layer of particulate contaminants from soil surfaces. In 1974 he joined the Theoretical Division's Fluid Dynamics Group to develop computational fluid-dynamics models for investigating reactor safety problems of specific interest to the Nuclear Regulatory Commission.